Mechanical mechanisms of the directional shift and inverse of the eccentric compound droplet

Jingtao Wang, Shen Xu, Yan Huang, and Jing Guan

Citation: Physics of Fluids **30**, 042005 (2018); doi: 10.1063/1.5024252
View online: https://doi.org/10.1063/1.5024252
View Table of Contents: http://aip.scitation.org/toc/phf/30/4
Published by the American Institute of Physics

Mechanical mechanisms of the directional shift and inverse of the eccentric compound droplet

Jingtao Wang,[1,a)] Shen Xu,[1] Yan Huang,[1] and Jing Guan[2,b)]
[1]*School of Chemical Engineering and Technology, Tianjin University, Tianjin 300072, People's Republic of China*
[2]*School of Mathematics, Tianjin University, Tianjin 300072, People's Republic of China*

(Received 30 January 2018; accepted 27 March 2018; published online 10 April 2018)

Mechanical mechanisms of the directional movement and inverse of an eccentric compound droplet in a modest extensional flow are investigated in this paper by spectral boundary element methods. In this work, a phenomenon is revealed that the shift of a compound droplet is driven by the asymmetric interfacial curvature, not just the outer drag. The asymmetric layout of the daughter droplet leads to the asymmetric drags from the continuous phase and the asymmetric deformation of the compound droplet with different interface curvatures. As the inner droplet has both enhancing and suppressing effects on the globule deformation (during different stages), the interface curvatures will vary when the relative size and location of the inner droplet are changed. The curvature difference results in the asymmetric pressure distribution and circulation inside the compound droplet. Eventually, the interaction of the inner driving force (curvature difference) and the outer drags results in the directional shift and inverse of the compound droplet. The shift direction is affected by the structural asymmetry parameter ε (eccentricity) and some flow features such as the capillary number. The conclusion could enlighten potential applications for the movement of soft globules driven by the curvature difference. *Published by AIP Publishing.* https://doi.org/10.1063/1.5024252

NOMENCLATURE

r_{MR}	initial radius of the globule
r_R	initial radius of the daughter droplet
d_R	initial distance between the two centroids
N_B	basis points
D	deformation parameter
Ca	capillary number
S_{11}	the interface of the globule
S_{21}	the interface of the daughter droplet
U	average velocity of the domain flows
F_x	outer drags of the globule in the x-axis
G	shear rate
G_0	the shear rate at the wall of the outlet when the volume flow rate $Q = 2R_0^2/3$
Q	volume flow rate
R_0	width of the outlet channel
u	velocity
f	surface stress
n	normal vector

Superscripts

mom	globule
CP	continuous phase

Greek symbols

ε	asymmetry parameter(eccentricity)
μ	viscosity
γ	interfacial tension
λ	viscosity ratio

I. INTRODUCTION

As complex soft particles, multiple-emulsion compound droplets are typical of skillfully designed internal structures.[1] Since they might have multiple engulfed independent droplets and thus sequentially broad potentials, they have drawn much attention recently in many fields such as the drug delivery, food, and cosmetics industry.[2] At most times, these complex compound droplets stored and delivered in the liquid phase always deform under the force of the flow shear. Thus, it is essential to study their rheological behaviors in more detail.

Up to now, many studies about the rheology of multiple-emulsion compound droplets especially for concentric double emulsions (CDEs) in different flow systems by using experiments[3–6] and numerical simulations[5,7–10] have been reported. The controlled release[3,4] and split[6] of double-emulsion compound droplets under the flow shear, located in three-dimensional microchannel assembled by capillary tubes, had been studied by a lot of experiments. Besides these experiments, the rheological behaviors of multiple-emulsion compound droplets have been studied with numerical methods by many researchers. As early as in 1990, Stone and Leal[7] studied the deformation and breakup of the CDE compound droplet in infinite extensional flows and therefore proposed two different breakup mechanisms. Chen *et al.*[5] investigated the effects of the inner droplet of CDEs on its deformation in shear flows. They demonstrated that there are two coexisting

[a)]wjingtao928@tju.edu.cn
[b)]guanjing@tju.edu.cn

enhancing and suppressing effects of the inner droplet on the deformation of the compound droplet when the deformation process reached an equilibrium.

Furthermore, the rheological behaviors of the multiple-emulsion compound droplet in straight and constriction tubes have been investigated by numerical simulations.[11–13] Through a spectral boundary element method (BEM), Wang *et al.*[13] simulated the translation process of double-emulsion compound droplets containing two unequal daughter droplets (DDs) in a constriction tube. It is very interesting that the required maximum pressure drop is relatively lower when the initial location of the bigger daughter droplet is in the front, which demonstrates that the compound droplet is easier to pass the constriction in this way.

Later, due to their potential applications in the controlled release of the compound droplet insertion, the rheological behaviors of multiple-emulsion compound droplets with complex asymmetric internal structures and the directional movement of their inner droplets have drawn much attention of some researchers. Wang and his co-workers[14–16] designed asymmetric multiple-emulsion compound droplets with three layers. In the second layer, there is one big DD which presented asymmetric internal structures. Because of the structural asymmetry in the third layer, the daughter droplet will shift in a certain direction, which will cause the directional contact of the outmost interface of the compound droplet and DD. Therefore, the compound droplet is able to be broken up and have directional release. Moreover, Wang *et al.*[16] indicated that the shift caused by the internal asymmetry is controlled not only by the asymmetric structures but also by the flow features such as the viscosity ratio and capillary number. The shift direction will be inversed by changing these factors. As for the eccentric compound droplet, Qu and Wang[17] have investigated its rheological behaviors in a planar extensional flow. They reported that the eccentric compound droplet will shift away in the same direction as the moving direction of the inner droplet. The speed of the compound droplet is proportional to the distance between two centers of the compound droplet and the inner droplet, i.e., proportional to the eccentricity. However, the phenomena and mechanism of the directional shift of the compound droplet have not been explored deeply in this work and would not present the physical explanations of the shift reverse.

In addition, Wang and co-workers studied the rheological behavior of a simple droplet in an asymmetric extensional flow.[18,19] In their studies, the droplet is symmetric, but the outer flow surrounding the drop is asymmetric. When the capillary number is small, the droplet could not break up and always shifts in the same direction in which the droplet suffers bigger outer drags from the continuous phase. However, for a multiple-emulsion compound droplet with an internal asymmetry in an extensional flow under modest capillary numbers, as the asymmetry is from the interior of the compound droplet, its shift might be more complex and will not be caused by only the outer drag.

The impact of compound droplets' internal asymmetry on the inner pressure distribution, interface curvature difference, and drags on the outer boundary of the compound droplet are investigated in this paper by boundary element methods. Compared to other numerical methods such as finite element methods (FEM),[20] finite volume methods (FVM),[21] and control-volume finite element methods (CVFEM),[22,23] the boundary element method (BEM) handles only the points on the boundary. Thus, it will reduce the problem dimensionality by one and is easy to treat the problem involving multiple interfaces like the problem treated in this paper.

II. MATHEMATICAL FORMULATION AND NUMERICAL METHOD

The rheological behaviors of a compound droplet [Figs. 1(b) and 1(d)] containing one eccentric daughter droplet in a modest extensional flow [Figs. 1(a) and 1(c)] are studied through a spectral boundary element method. The calculation is done in a two-dimensional case [Figs. 1(a) and 1(b)], but it is equivalent to an axisymmetric case [Figs. 1(c) and 1(d)].

As illustrated in Fig. 1(b), the daughter droplet (DD) is located on the x-axis. The initial radii of the compound droplet and daughter droplet are r_{MR} and r_R, respectively, and d_R is the distance between the two centroids at the initial time. We define the asymmetry as $\varepsilon = d_R/(r_{MR} - r_R)$. The interface of compound droplet is S_{11}, and the inner interface is S_{21}. The DD filled with an inner phase with viscosity μ, the room between the compound droplet and DD filled with an outer phase with viscosity μ_1, the compound droplet suspended in a modest extensional flow with viscosity μ. The three phases of fluid are assumed incompressible, Newtonian, and immiscible with each other. According to the work of Wang *et al.*,[16] several factors affect the directional shift of the compound droplet. One is the defined asymmetry ε and the other one is the capillary number Ca. $Ca = \mu U/\gamma$, where $U = 1$ is the average velocity of the domain flows (continuous phase) at inlets, $\mu = 1$ is the viscosity of the domain flows, and γ is the interfacial tension. γ will be changed to adjust the value of Ca. Meanwhile, we also investigate the x component of outer drags $\boldsymbol{F_x}$ of the compound droplet and its internal pressure distribution to reveal mechanism of the directional shift of the compound droplet.

According to the work of Wang *et al.*,[14,15] the corresponding boundary conditions are given in the following. The non-slip microchannel boundary condition is $u_0 = 0$. The flow at the inlet and outlet of the microchannel is driven by pressure, whose parabolic velocity profile is

$$u_0 = \pm G\frac{R_0}{2}\left[1 - \left(\frac{R}{R_0}\right)^2\right]\mathbf{n}, \tag{1}$$

where G is the shear rate, the negative sign is for the outlets and the positive sign is for the inlets, and $\mathbf{n}$ is the normal vector.

All physical quantities here are dimensionless and reduced by some scale, we employ the radius $R_0 = 1$ of the outlet channel as the length scale. G_0 is the shear rate at the wall of the outlet when the volume flow rate $Q = 2{R_0}^2/3$, ${G_0}^{-1}$ is the time scale, and $\mu_0 G_0$ is the pressure scale. The viscosity and the interface tension are scaled by μ_0 and $\mu_0 R_0 G_0$, respectively. Initially, all droplets are spherical due to surface tensions. The radius of the compound droplet $r_{MR} = 0.5R_0$ and that of $r_R = 0.1R_0$.

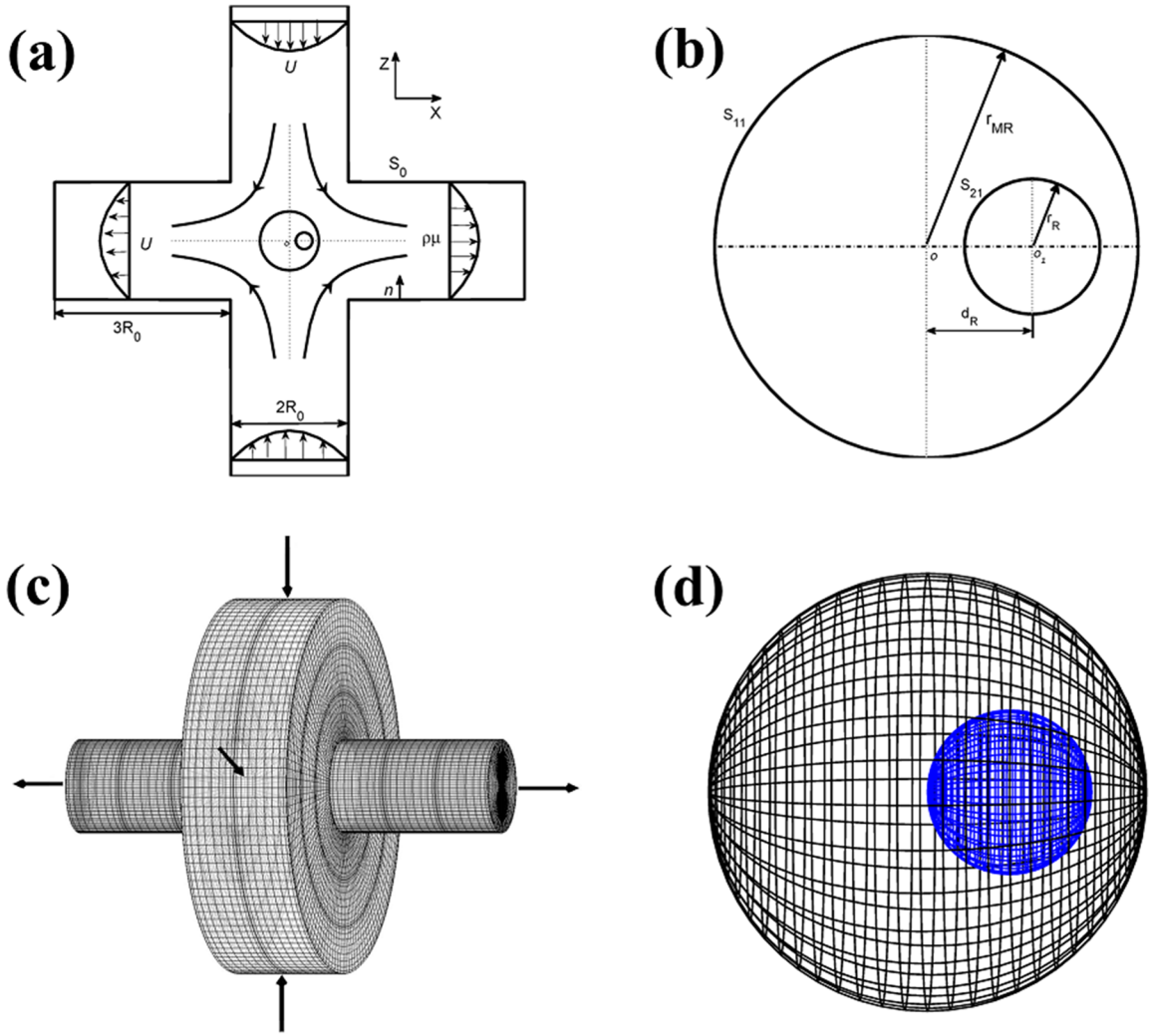

FIG. 1. [(a) and (b)] The illustration of the 2-dimensional cross-like microfluidic device and eccentric double-emulsion compound droplet. [(c) and (d)] The illustration of the equivalent axisymmetric cross-like microfluidic device and axisymmetric multiple-emulsion compound droplet.

The size of the microchannel (10^{-6} m) is in the micron scale. The Stokes equation and continuity equation as the governing equation are employed in our system with incompressible low-Reynolds number flow,

$$\nabla \cdot \mathbf{u} = 0, \tag{2}$$

$$-\nabla p + \mu \nabla^2 u = 0, \tag{3}$$

where μ is the viscosity for each phase, p is the dynamical pressure, and u is the velocity.

On the interfaces (S_{11} and S_{21}) of the compound droplet,

$$\begin{cases} u_{2,1} = u_{2,1}^{mom} \\ u_{1,1} = u_{1,1}^{CP} \end{cases},$$

$$\begin{cases} \Delta f_{1,1} = f_{1,1}^{CP} - f_{1,1} = \gamma_{1,1}(\nabla \cdot n)n + \left(\kappa_{1,1}^{CP} - \kappa_{1,1}\right)\rho\,(g \cdot x)\,n \\ \Delta f_{2,1} = f_{2,1}^{mom} - f_{2,1} = \gamma_{2,1}(\nabla \cdot n)n + \left(\kappa_{2,1}^{mom} - \kappa_{1,1}\right)\rho\,(g \cdot x)\,n \end{cases}. \tag{4}$$

The superscripts "mom" and "CP" indicate the mother droplet and continuous phase, respectively. $f_{2,1}$ is the surface stress of the inner side of the surface S_{21}, and $f_{2,1}^{mom}$ is the surface stress of the outer side of the surface S_{21}. Because the microchannel is in micron size and the surface tensions play a major role, the effects of gravities and buoyancies are negligible.

LHS is defined as

$$LHS = \begin{cases} 2\pi\mu \boldsymbol{u}(\boldsymbol{x}_0), & \boldsymbol{x}_0 \in S_0, \\ 2\pi\mu(1+\lambda_{1,1})\boldsymbol{u}(\boldsymbol{x}_0), & \boldsymbol{x}_0 \in S_{1,1}, \\ 2\pi\mu(\lambda_{1,1}+\lambda_{2,1})\boldsymbol{u}(\boldsymbol{x}_0), & \boldsymbol{x}_0 \in S_{2,1}. \end{cases} \tag{5}$$

The velocity at a point $\boldsymbol{x}_0$ on the interface including boundary S_0 and the surface of the droplet S_{11} and S_{21} could be expressed as the following integral of the velocity and surface stress f:

$$\begin{aligned} LHS = &-\int_{S_0} [\boldsymbol{S} \cdot \boldsymbol{f} - \mu \boldsymbol{T} \cdot \boldsymbol{u} \cdot \boldsymbol{n}] dS \\ &-\int_{S_{1,1}} [\boldsymbol{S} \cdot \Delta \boldsymbol{f}_{1,1} - (1-\lambda_{1,1})\mu \boldsymbol{T} \cdot \boldsymbol{u} \cdot \boldsymbol{n}] dS \\ &-\int_{S_{2,1}} [\boldsymbol{S} \cdot \Delta \boldsymbol{f}_{2,1} - (\lambda_{1,1}-\lambda_{2,1})\mu \boldsymbol{T} \cdot \boldsymbol{u} \cdot \boldsymbol{n}] dS. \end{aligned} \tag{6}$$

The fundamental solutions for the two-dimensional Stokes flow are[24,25]

$$\boldsymbol{S}_{ij}(\hat{\boldsymbol{x}}) = -\delta_{ij}\ln r + \frac{\hat{x}_i\hat{x}_j}{r^2}, \tag{7}$$

$$\boldsymbol{T}_{ijk}(\hat{\boldsymbol{x}}) = -4\frac{\hat{x}_i\hat{x}_j\hat{x}_k}{r^4}. \tag{8}$$

The vector $\hat{\boldsymbol{x}}$ is defined as $\hat{\boldsymbol{x}} = \boldsymbol{x} - \boldsymbol{x}_0$, and $r = |\hat{\boldsymbol{x}}|$. These fundamental solutions describe the flow induced by stress at point $\boldsymbol{x}_0$.

The following two integral equations could be used to calculate the velocities at any interior points,

$$2\pi\mu\boldsymbol{u}(\boldsymbol{x}_0) = -\int_B [\boldsymbol{S}\cdot\boldsymbol{f} - \mu\boldsymbol{T}\cdot\boldsymbol{u}\cdot\boldsymbol{n}]dS, \tag{9}$$

$$-\int_B [\boldsymbol{S}\cdot\boldsymbol{f} - \mu\boldsymbol{T}\cdot\boldsymbol{u}\cdot\boldsymbol{n}]dS = \begin{cases} 4\pi\mu\lambda\mathbf{u}(\boldsymbol{x}_0), & \boldsymbol{x}_0 \in \mathrm{DP} \\ 4\pi\mu\mathbf{u}(\boldsymbol{x}_0), & \boldsymbol{x}_0 \in \mathrm{CP} \end{cases}. \tag{10}$$

$4\pi\mu\lambda\mathbf{u}(\boldsymbol{x}_0)$ is for $\boldsymbol{x}_0$ in the interior of the compound droplet (dispersed phase) and $4\pi\mu\mathbf{u}(\boldsymbol{x}_0)$ is for $\boldsymbol{x}_0$ in the interior of the domain (continuous phase).

The following pressure distribution equation was employed to determine the pressure at any point $\boldsymbol{x}_0$:

$$\begin{aligned} 4\pi p(x_0) = &-\int_{S_0} [\boldsymbol{P}\cdot\boldsymbol{f} - \mu\boldsymbol{\Pi}\cdot\boldsymbol{u}\cdot\boldsymbol{n}]dS \\ &-\sum_{\mathrm{j}=1}^{\mathrm{m_1}}\int_{S_{1,1}} [\boldsymbol{P}\cdot\Delta\boldsymbol{f}_{1,1} - (1-\lambda_{1,1})\mu\boldsymbol{\Pi}\cdot\boldsymbol{u}\cdot\boldsymbol{n}]dS \\ &-\sum_{\mathrm{i}=2}^{\mathrm{n}}\sum_{\mathrm{j}=1}^{\mathrm{m_i}}\int_{S_{\mathrm{i},2}} [\boldsymbol{P}\cdot\Delta\boldsymbol{f}_{1,2} - (\lambda_{1,1}-\lambda_{2,1})\mu\boldsymbol{\Pi}\cdot\boldsymbol{u}\cdot\boldsymbol{n}]dS. \end{aligned} \tag{11}$$

The fundamental solution for two-dimensional pressure field is expressed as

$$\boldsymbol{P}_i = 2\frac{\hat{x}_i}{r^2}, \tag{12}$$

$$\boldsymbol{\Pi}_{ik}(\boldsymbol{x}_0, \boldsymbol{x}) = 2\left(-\frac{\delta_{ik}}{r^2} + 2\frac{\hat{x}_i\hat{x}_k}{r^4}\right), \tag{13}$$

where $\hat{\boldsymbol{x}} = \boldsymbol{x} - \boldsymbol{x}_0$, $r = |\hat{\boldsymbol{x}}|$, $\boldsymbol{x}_0$ is the reference point, and $\boldsymbol{x}$ is an arbitrary point in the local region.

The validation of this numerical method has been well done in our previous papers.[15] For problems with smooth boundary, the boundary of the compound droplet is discretized into $\mathrm{N_E}$ section according to the spectral boundary element methods. The geometric variables on each element can be obtained by the higher order expansion of orthogonal polynomials using the local variables on interval [−1, 1]. The number of $\mathrm{N_B}$ spectral points on each element is corresponding to the roots of Jacobi polynomials of order $\mathrm{N_B}$. Meanwhile, the parameter of boundary integral equation could be discretized, and a linear system of algebraic equation is formed

$$\boldsymbol{u} = \boldsymbol{A}\boldsymbol{f} + \boldsymbol{B}\boldsymbol{u}. \tag{14}$$

The matrices **A** and **B** are obtained by the integration of the kernels **S** and **T**. Gauss quadrature with Legendre and Lobatto points are employed for the integrations. Gauss elimination is then used to solve the linear system for the velocity and stress.

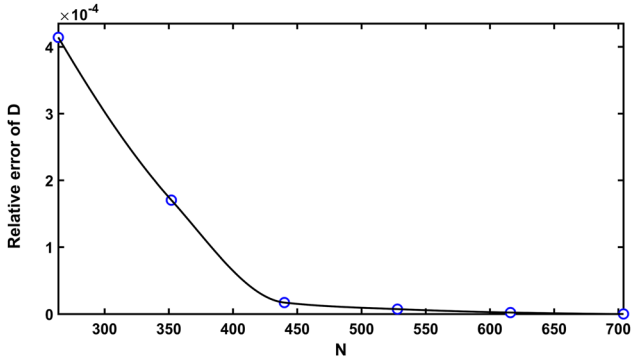

FIG. 2. The relation between the total points number N and the relative error of deformation D.

A simple droplet in a flow system with appropriate parameter is employed to verify the convergence of our numerical method. For this system, the deformation parameter D when the droplet reaches an equilibrium is chosen to evaluate the most appropriate basis points $\mathrm{N_B}$. The total number $\mathrm{N_E}$ of elements is 44, and basis points $\mathrm{N_B}$ = 6, 8, 10, 12, 14, and 16 are changing for each element. Results for $\mathrm{N_B}$ = 16 are used as the exact D in the calculation of the relative error. In this investigation, when N = 44 * $\mathrm{N_B}$ = 440, the relative error is lower than 10^{-4}, and when N is larger than 440 the relative error changes a little. Thus, we employ $\mathrm{N_B}$ = 10 to ensure the calculation accuracy and to reduce computing time. It could be seen in Fig. 2 which is about the variation of relative error under different N.

III. RESULTS AND DISCUSSIONS

In the investigated flow system, when taking the compound droplet interface as the boundary, the continuous phase surrounding the compound droplet is the outer flow; the dispersed phase between the interfaces of the compound droplet and the daughter droplet is the inner flow. Thus, the entire flow field is divided into two regions: the outer flow which could generate drags to the compound droplet and the inner circulation which could result in the movement of the mass center of the compound droplet. Apparently, the asymmetric layout of the daughter droplet would cause an asymmetric pressure distribution and a directional circulation inside the compound droplet (see Fig. 3). Thus, the compound droplet might shift in some specific direction (to the left or right), and the direction is determined by both the internal asymmetry and some flow characteristic parameters such as Ca. As shown in Fig. 3, under the same $Ca = 0.2$, double-emulsion compound droplets with different initial eccentricities have opposite pressure distributions and inner circulation and further have the opposite shift direction.

It is well known that the inner circulation has four symmetric eddies when a concentric compound droplet or a simple droplet reaches the equilibrium. However, for the eccentric compound droplet, it will not have an equilibrium state since it will move away from its initial location. Nevertheless, according to the pattern of the inner circulation of the eccentric

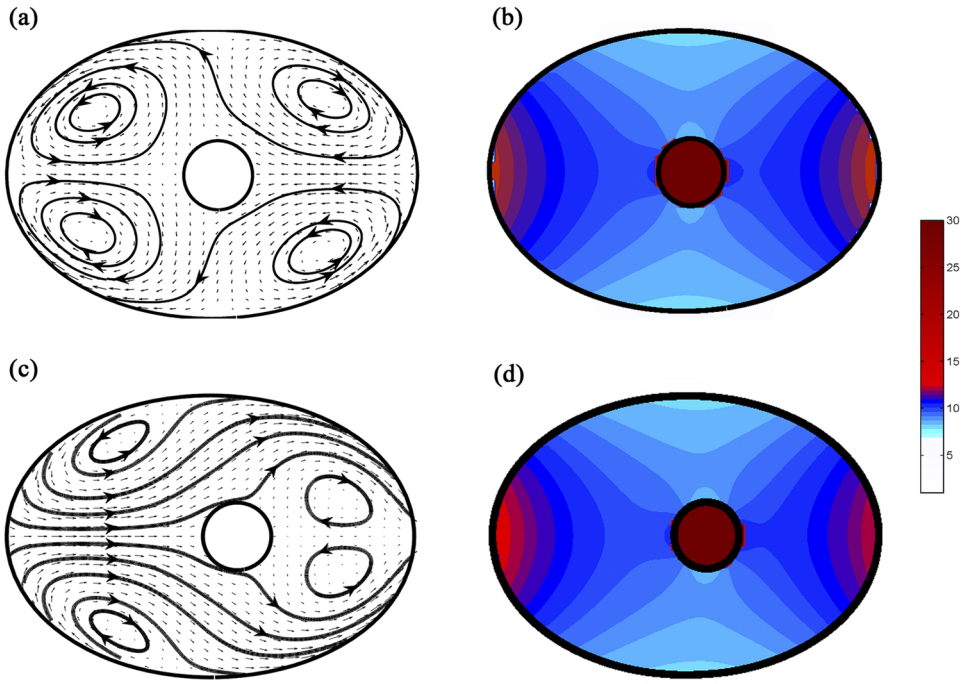

FIG. 3. [(a) and (b)] When the initial $\varepsilon = 0.375$ and $Ca = 0.2$, the eccentric compound droplet will shift to the left due to the asymmetric internal circulation and pressure distribution. [(c) and (d)] When the initial $\varepsilon = 0.750$ and $Ca = 0.2$, the same compound droplet will shift to the right due to the asymmetric internal circulation and pressure distribution.

compound droplet (see Fig. 4), the process could also be divided into two stages: before the formation of the circulation with four eddies (BF, t = 0 to about t = 1) and after that (AF). At time t = 1.0, four steady eddies in the circulation have almost been generated as shown in Fig. 4(b). In the AF stage, according to displacement of the compound droplet mass center, the deformation could also be separated into two stages: unclear displacement (AFUD, about t = 1 to about t = 4) and clear displacement (AFCD, about t > 4). In the AFUD stage, the compound droplet has clear displacement and its inner circulation has four steady eddies [see Fig. 4(c)]; in the AFCD stage, the mass center of the compound droplet moves away from its initial location significantly and it could be seen that the liquid inside the droplet moves from the right to the left through the inner circulation [see Fig. 4(d)]. The patterns of the inner circulation for eccentric compound droplets with different initial eccentricities ε are almost the same.

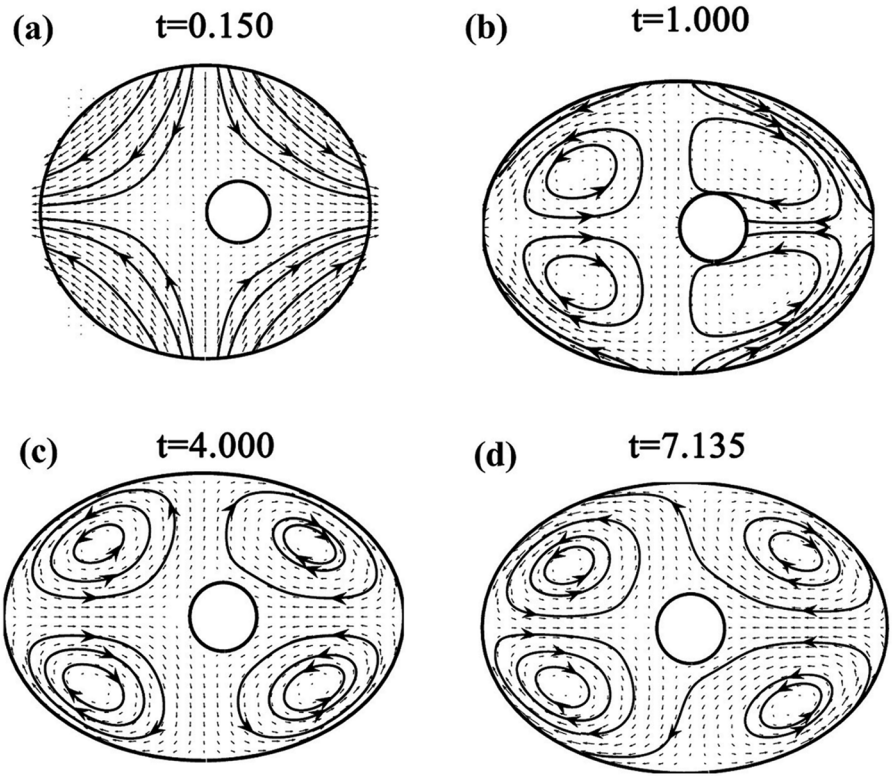

FIG. 4. The inner circulations of eccentric compound droplet with $\varepsilon = 0.375$ and $r_R = 0.1R_0$ at different stages.

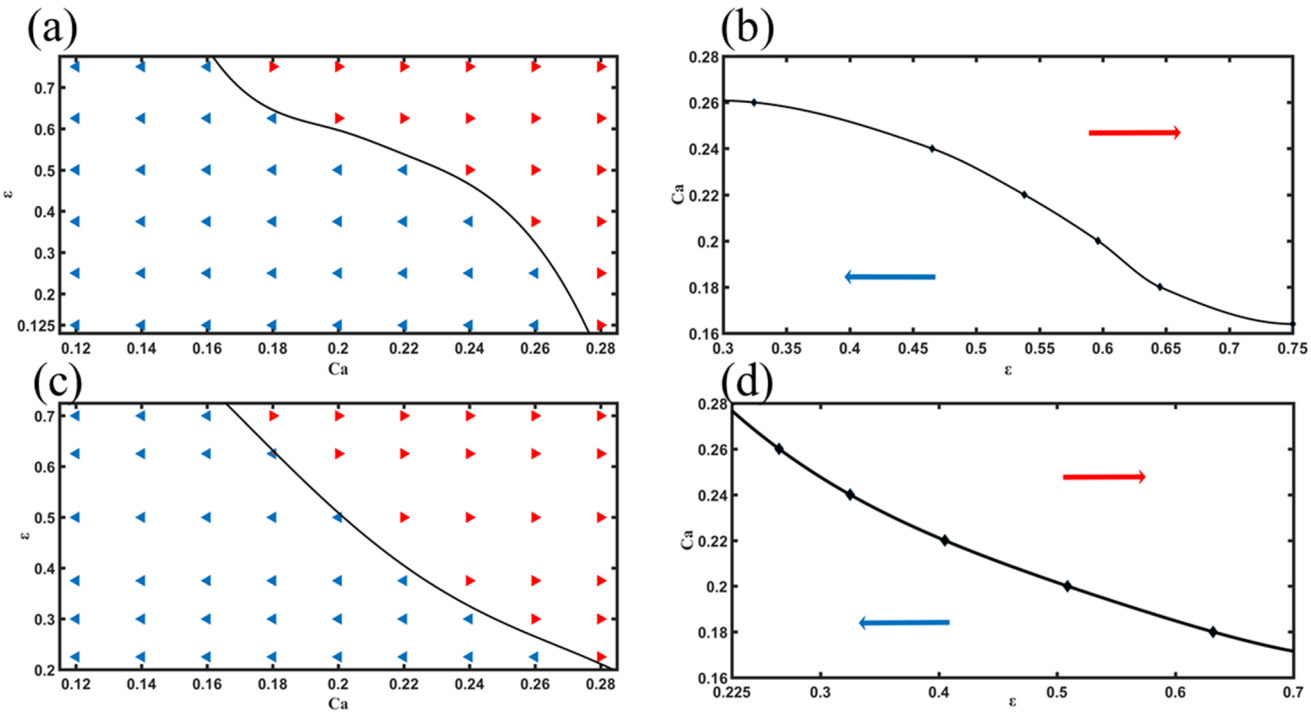

FIG. 5. Regimes of the shift direction in terms of ε and Ca [(a) and (c)], and the critical capillary number as a function of ε [(b) and (d)]. For (a) and (b), $r_R = 0.1R_0$ is fixed and the initial ε changes through the variation of the eccentric distances d_R. For (c) and (d), $d_R = 0.1R_0$ is fixed and the initial ε changes through the variation of the inner droplet radius r_R.

As shown in Fig. 5, the regimes of the shift direction in terms of ε and Ca for two cases have been investigated. In the first case [Figs. 5(a) and 5(b)], $r_R = 0.1R_0$ is fixed and the initial ε changes through the variation of the eccentric distances d_R; in the second case [Figs. 5(c) and 5(d)], $d_R = 0.1R_0$ is fixed and the initial ε changes through the variation of the inner droplet radius r_R. For both the cases [Figs. 5(a) and 5(c)], when ε and Ca are relatively small, the compound droplet generally shifts to the left; when ε and Ca are relatively large, it will shift to the right. The critical capillary numbers as functions of ε are shown in Figs. 5(b) and 5(d), respectively. It could see that the larger the initial ε is, the smaller the critical capillary number is. Below the curve of critical capillary numbers, the droplet will move to the left; above the curve, the droplet will move to the right.

In order to see more details of the shift and inverse, the displacement d of the mass center of the eccentric compound droplets along with time at various capillary numbers and initial eccentricities is explored and shown in Fig. 6. Figures 6(a) and 6(b) come from Fig. 5(a) when Ca = 0.16 and 0.20, respectively; Figs. 6(c) and 6(d) come from Fig. 5(c) when Ca = 0.16 and 0.20, respectively. When the initial ε is changed from 0.125 to 0.750 through the variation of the eccentric distances d_R, the capillary number is 0.16 for Fig. 6(a) and is 0.20 for Fig. 6(b). Comparing Figs. 6(a) and 6(b), it is obvious that the shift behaviors of the same eccentric compound droplet under two capillary numbers are different. As for Fig. 6(a), the eccentric compound droplet intends to shift to the left when the initial eccentricities vary from 0.125 to 0.750. However, although the compound droplet always shifts to the left in this case, the shift speed is not monotonically increasing [see Fig. 7(a)]. From ε = 0.125 to 0.375, the speed of shift to the left increases; however, from ε = 0.375 to 0.750, the speed decreases continuously. As for Fig. 6(b), the eccentric compound droplet might shift either to the left or to the right when the initial ε is in the range from 0.125 to 0.750. From ε = 0.125 to 0.375, the compound droplet shifts to the left and its speed increases; from ε = 0.375 to 0.500 the compound droplet shifts to the left but its speed decreases [see Fig. 7(b)]. When the initial eccentricities are 0.625 and 0.750, the shift direction of the compound droplet changes to the right and the speeds increase [see Fig. 7(b)]. When the initial ε is changed from 0.225 to 0.700 through the variation of the inner droplet radius r_R, the capillary number is 0.16 for Fig. 6(c) and is 0.20 for Fig. 6(d). Comparing Figs. 6(c) and 6(d), it could also be seen that the shift behaviors are different for the same eccentric compound droplet under various capillary numbers. As for Fig. 6(c), the eccentric compound droplet always tends to move to the left when the initial eccentricity varies in the range of 0.225–0.700. However, its shift speed is also not monotonically increasing [see Fig. 7(c)]: from ε = 0.225 to 0.375, the shift speed increases; from ε = 0.375 to 0.700, the speed decreases. As for Fig. 6(d), the eccentric compound droplet could shift either to the left or to the right. When the initial ε varies from 0.200 to 0.375, the compound droplet shifts to the left and its speed increases; from ε = 0.375 to 0.500, the compound droplet shifts to the left but its speed decreases continuously [see Fig. 7(d)]. When the initial ε is increased to 0.700, the compound droplet inverses its shift direction and moves to the right. From the above analysis, it could be asserted that the relatively small initial eccentricity and its appropriate increase will benefit the shift to the left; however, when beyond a limit, the increment of the eccentricity is beneficial to the left shift no longer and might benefit the shift to the right when

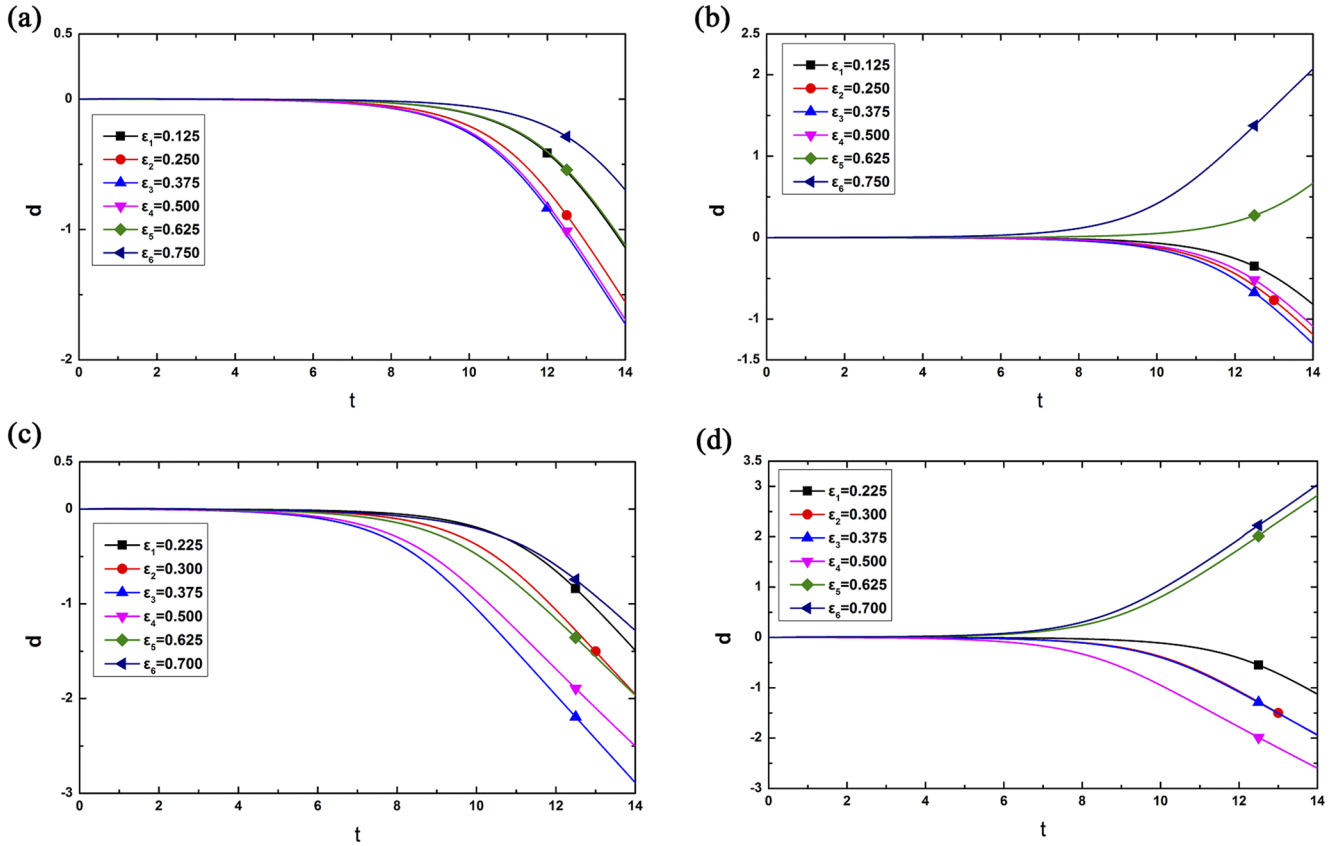

FIG. 6. The displacement of the mass center of the compound droplets with one eccentric daughter droplet along with time at various initial eccentricities and capillary numbers [$Ca = 0.16$ for (a) and (c); $Ca = 0.20$ for (b) and (d)]. For figure (a) and (b), $r_R = 0.1R_0$ is fixed and the initial ε changes through d_R. For figure (c) and (d), $d_R = 0.1R_0$ is fixed and the initial ε changes through r_R.

the initial ε is big enough. In addition, from Fig. 6, we also could know that the relatively large *Ca* is beneficial to the right shift.

In order to explain the phenomena shown in Fig. 6(b), Fig. 6(b) has been analyzed further, and the corresponding explorations are shown in Figs. 8–10, respectively. At first, the

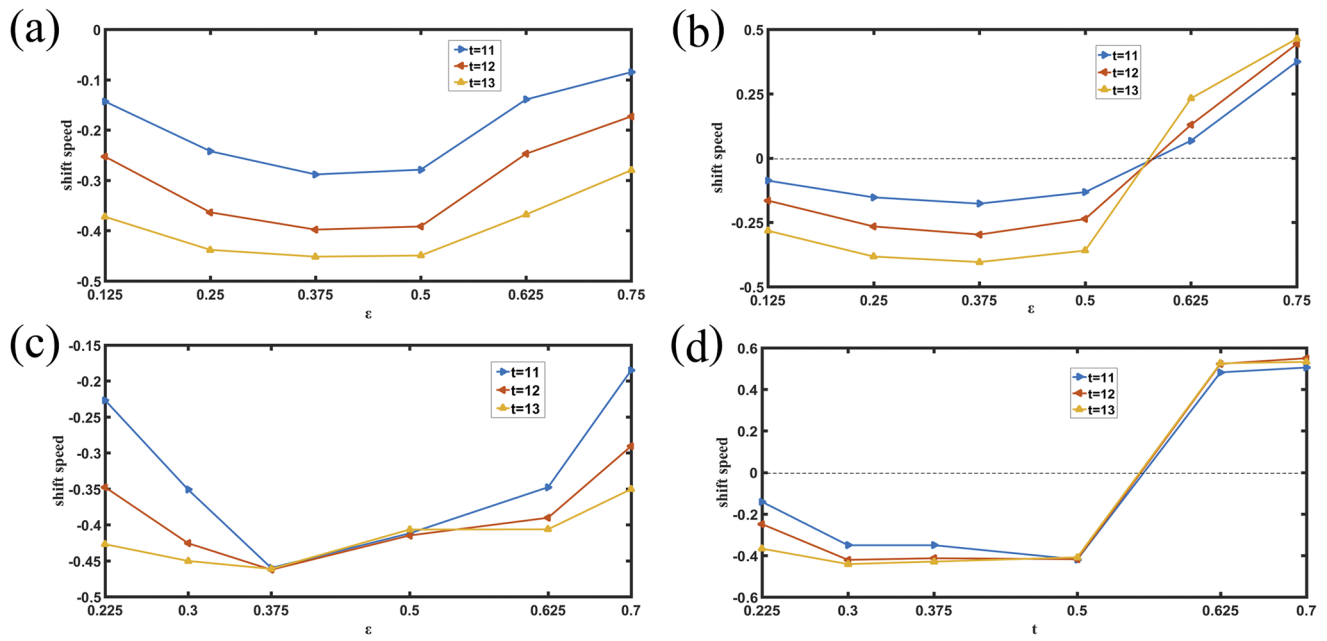

FIG. 7. The speed variation of the mass center of the compound droplets along with the change of ε at time t = 11, 12, and 13. The four figures, (a)–(d), correspond to Figs. 6(a)–6(d), respectively.

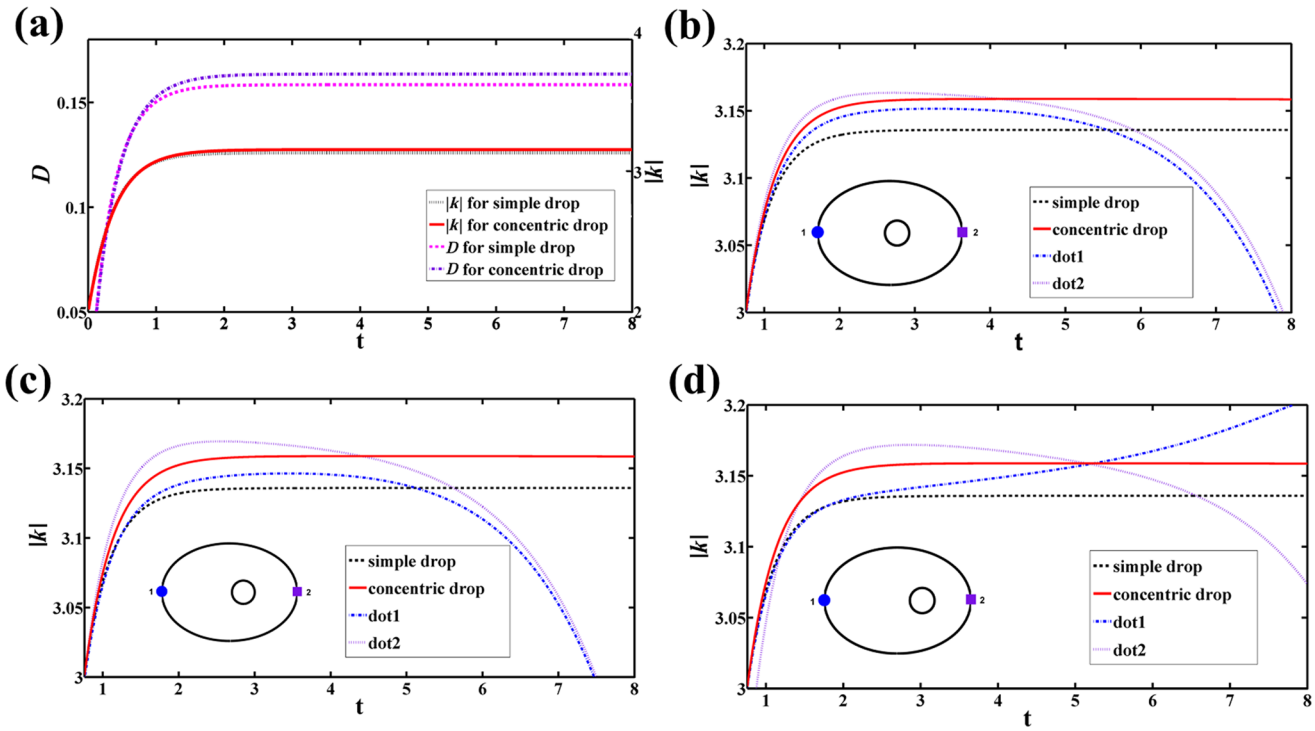

FIG. 8. The deformation parameter D and interfacial curvatures (absolute values $|k|$) at two ends of the compound droplets *versus* time t for the simple drop, concentric compound droplet, and eccentric compound droplet under $Ca = 0.2$. (a) D and $|k|$ *versus* t for the simple drop and concentric compound droplet. $|k|$ *versus* t for eccentric compound droplet with initial $\varepsilon = 0.125$ (b), $\varepsilon = 0.375$ (c), and $\varepsilon = 0.750$ (d).

interfacial curvatures k at the right and the left endpoints of the deformed compound droplet are explored and shown in Fig. 8. When the inner droplet is exactly staying at the center of the compound droplet, we have a concentric compound droplet whose eccentricity ε is zero. As shown in Fig. 8(a), when the deformation reaches an equilibrium, both the deformation

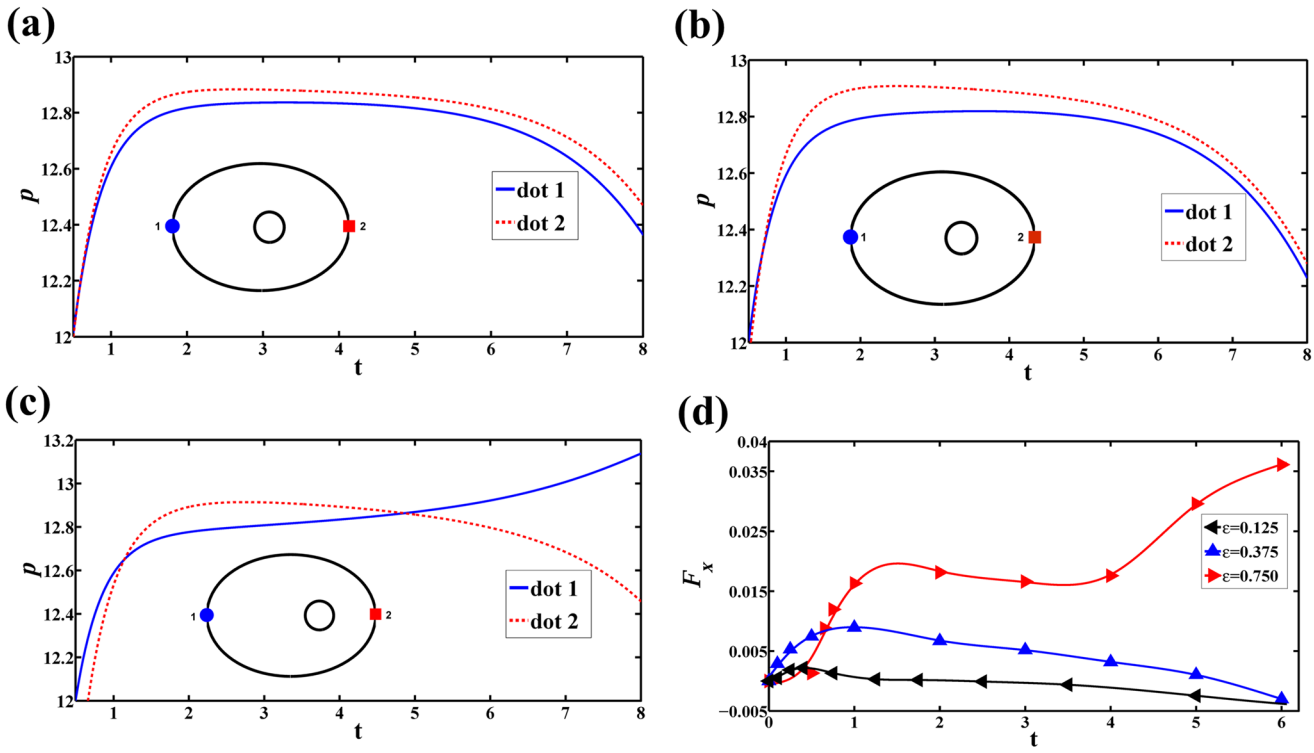

FIG. 9. The inner pressure p at two ends of the eccentric compound droplets *versus* time t for the initial eccentricity $\varepsilon = 0.125$ (a), $\varepsilon = 0.375$ (b), and $\varepsilon = 0.750$ (c) under $Ca = 0.20$. (d) The x component of the total drag force F_x *versus* time t for eccentric compound droplets with different initial eccentricities.

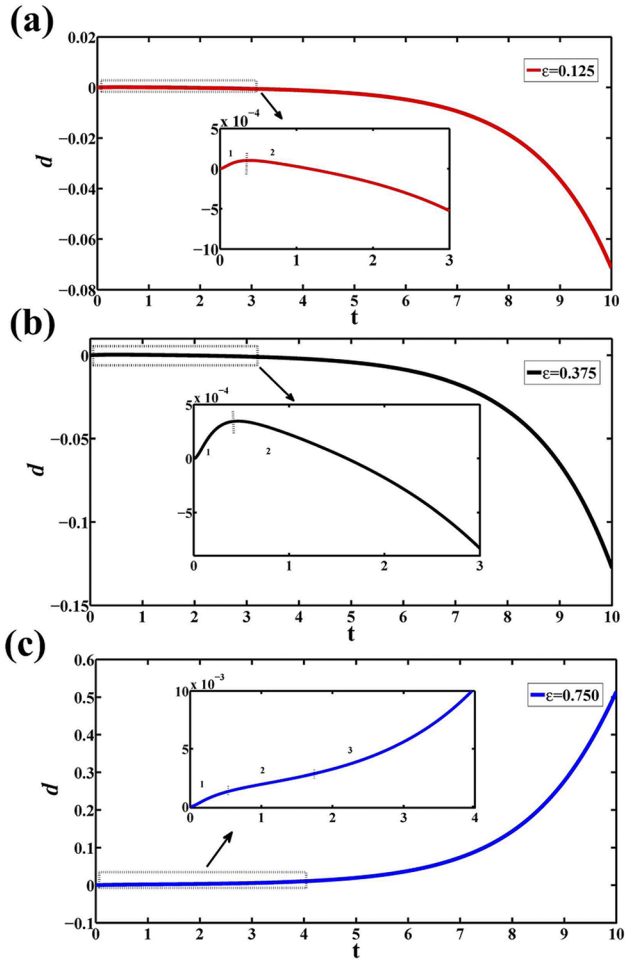

FIG. 10. The displacement d of the mass center of the eccentric compound droplets *versus* time t for various initial eccentricities under Ca = 0.20. (a) ε = 0.125, (b) ε = 0.375, and (c) ε = 0.750.

parameter D defined according to the reference papers[24,25] and the curvature for the concentric compound droplet are bigger than those for the simple droplet, which means the inner droplet will enhance the deformation at equilibrium period. As our interest focuses on the physical cause of the directional shift, we will concentrate on BF and AFUD stages since the AFCD stage is the result not the origin. As shown in Figs. 8(b)–8(d), due to the compound droplet eccentricity, the curvature at the left endpoint (dot 1) is different from that at the right endpoint (dot 2). In order to show the effects of the inner droplet on the interfacial curvatures, the curvature curves for the simple droplet and the concentric compound droplet are also shown in Figs. 8(b)–8(d) as contrasts. In the AFUD stage, it is obvious that the curvature at dot 2 is larger than that for the concentric compound droplet since the inner droplet is closer to dot 2 and thus has a stronger enhancing effect. Also, the curvature at dot 1 is less than that for the concentric compound droplet, but still larger than that for the simple droplet. This is reasonable since the inner droplet in eccentric compound droplets is farther to dot 1 than that in the concentric compound droplet and thus has a weaker enhancing effect. However, in the BF stage, the situation is just opposite. Although the difference might be very small when the eccentricity is low, it could still assert that the inner droplet has suppressing effects for the compound droplet deformation in the BF stage. It could be seen that in this stage the curvature at dot 1 is larger than that at dot 2 at the same moment, which is much clearer when the eccentricity is high.

The enhancing and suppressing effects of the inner droplet on the interfacial curvatures could also be seen in the pressure curves [Figs. 9(a)–9(c)] of two endpoints of the eccentric compound droplets. For the three different initial eccentricities ε = 0.125 [Fig. 9(a)], ε = 0.375 [Fig. 9(b)] and ε = 0.750 [Fig. 9(c)], the pressures at dot 1 are always higher than those at dot 2 in the BF stage, which could cause the right shift of the compound droplet; and in the AFUD stage, the pressures at dot 1 are always lower than those at dot 2, which could cause the left shift. Meanwhile, in the AFCD stage, the pressures at dot 1 are always lower for ε = 0.125 and ε = 0.375, which is consistent to the obvious shift of the compound droplet to the left; as for ε = 0.750, the situation is just opposite at most times, which is consistent to the obvious shift of the compound droplet to the right. In order to reveal the mechanism behind the oriented shift, the curves of the x component F_x of the sum drag forces for three eccentricities are shown in Fig. 9(d). Since the flow system is symmetric in the y direction, the y component F_y is always zero. When ε = 0.125 and ε = 0.375, values of F_x are positive (which means that the force points to the right) and increase along with time at the BF stage. Then, when F_x reaches a maximum value, the curves will decline along with time, and in the AFCD stage they might have negative values. When ε = 0.750, values of F_x are always positive and much higher than those for ε = 0.125 and ε = 0.375 at most of the time. In the BF stage, the curve of F_x ascends rapidly; in the AFUD stage, values of F_x are relatively quite large but do not change very much; in the AFCD stage, the curve of F_x ascends along with time again. From the above analysis, it could be seen that the outer drag is generally stronger to the half of the eccentric compound droplet in which the inner droplet is staying. Furthermore, since the inner droplets always stay in the right half of the compound droplet for the cases studied in this paper, it could be asserted that the outer drags always tend to pull the compound droplet to the right in both BF and AFUD stages no matter how big the initial eccentricities are.

In order to see the effects of inner pressure differences and outer drag forces on the shift of the eccentric compound droplets further, the time-evolution curves of the mass center of the compound droplets are shown in Fig. 10, and the curves for both BF and AFUD stages are particularly magnified. When ε = 0.125 and ε = 0.375 [see Figs. 9(a) and 9(b)], initially, the compound droplets shift to the right a little bit, which is the actively combined action of the inner pressure differences and outer drag forces. Then, the curves of d descend continuously, which means that the compound droplets begin to shift to the left. At this moment, it could see from Figs. 10(a)–10(c) that the outer drags pull the compound droplet to the right but the inner pressure differences move the compound droplet to the left. Thus, it could be asserted that the left shifts of the eccentric compound droplets are caused by the inner pressure differences, i.e., by the interfacial curvature differences. When ε = 0.750 [see Fig. 10(c)], the d curve is always positive and ascends continuously although the ascending rates in different stages change a little bit. As shown in the inset of Fig. 10(c),

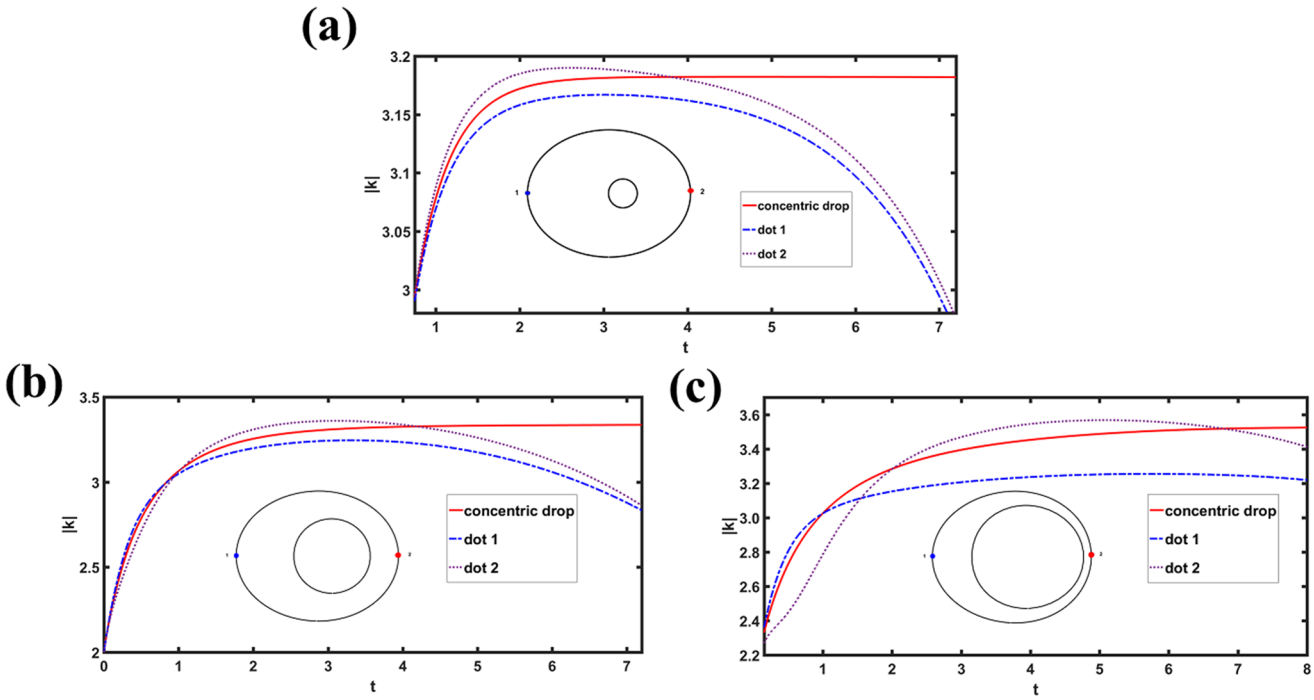

FIG. 11. Interfacial curvatures (absolute values |k|) |k| *versus t* for the eccentric compound droplet and corresponding concentric compound droplet with different initial eccentricities under $Ca = 0.20$. ε = 0.225 (a), ε = 0.375 (b), and ε = 0.700 (c).

the ascending rate in stage one is relatively high since both the inner pressure difference and the outer drag are positive to the right shift in this stage; in stage two, the outer drag is quite big and positive but the inner pressure difference [which is diminishing quickly, see Fig. 10(c)] is negative to right shift; thus, the slope of *d* curve in this stage decreases a little. In stage three, the inner pressure difference and the outer drag are both positive to the right shift again. Thus, we could assert that the right shift of the eccentric compound droplet is caused by the outer drag. The investigation in Figs. 8–10 only focuses on the cases shown in Fig. 6(b), in which the initial ε changes through the variation of the eccentric distances d_R.

The corresponding results shown in Fig. 6(d) are similar to those in Fig. 6(b). In order to explain the phenomena

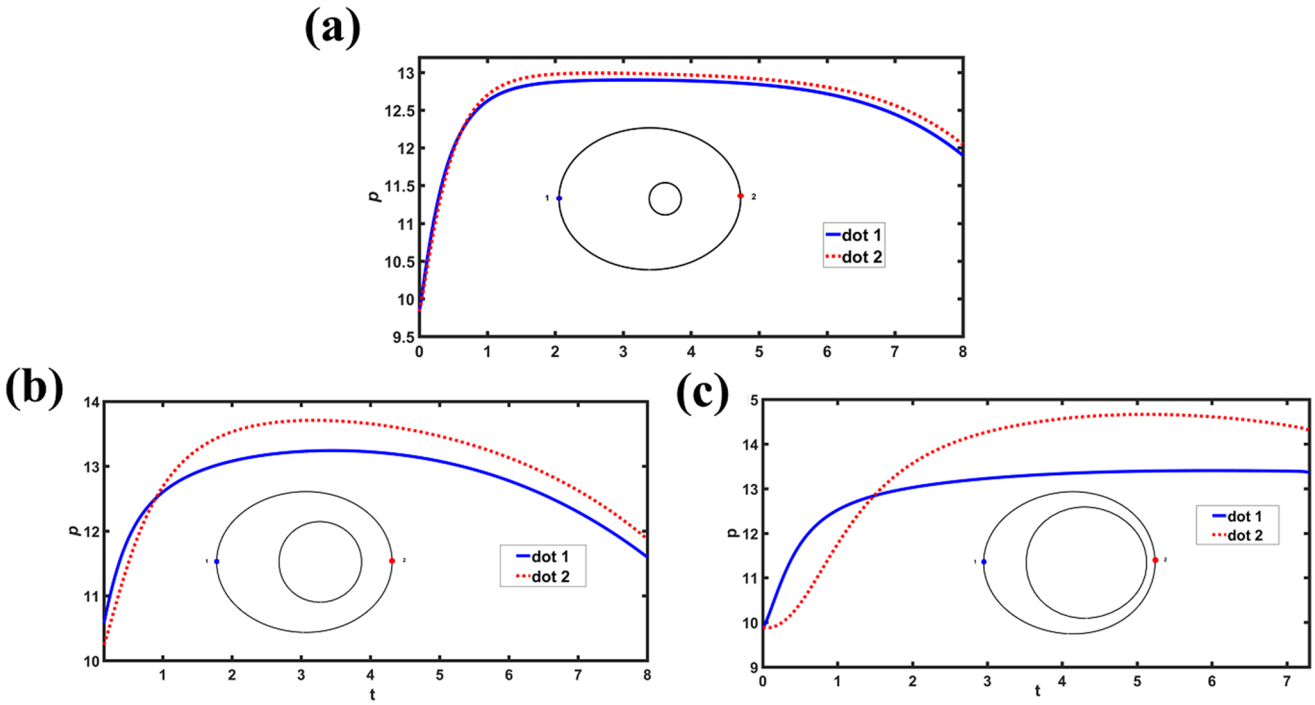

FIG. 12. The inner pressure *p* at two endpoints of the eccentric compound droplets *versus* time *t* for the initial eccentricity ε = 0.225 (a), ε = 0.375 (b), and ε = 0.700 (c) under $Ca = 0.2$.

(variation with the r_R), Fig. 6(d) has been analyzed further and the obtained results are shown in Figs. 11–14, respectively. From Fig. 6(d), the velocity of the compound droplet shift to the left increases as the relatively small initial eccentricity increase and reverses as it comes to the limit of the eccentricity. It could be asserted that the relatively small initial eccentricity and its appropriate increase will benefit the shift to the left; however, when beyond a limit, the increment of the eccentricity is beneficial to the left shift no longer and might benefit the shift to the right when the initial ε is big enough.

At first, the interfacial curvatures k at the right and left endpoints of the deformed compound droplet are investigated and shown in Fig. 11. Due to the inner eccentric droplet, the curvature at dot 1 is different from that at dot 2. In order to observe the effect of the volume of the daughter droplet on the interfacial curvatures, the curvature curves for the concentric compound droplets with the same size inner droplets as the eccentric compound droplets are also shown in Figs. 11(a)–11(c), respectively. In the AFUD stage (t = 1 − 4 s), since the inner droplet is closer to dot 2 and has a stronger enhancing effect, the curvature at dot 2 is larger than that for the concentric compound droplet; since the inner droplet in eccentric compound droplets is farther to dot 1 than that in the concentric compound droplet and has a weaker enhancing effect, the curvature at dot 1 is less than that for the concentric compound droplet. However, in the BF stage, the situation is opposite and the inner compound droplet has suppressing effects for the compound droplet deformation. In this stage, the curvature at dot 1 is larger than that at dot 2, and the difference is relatively big when the eccentricity is high.

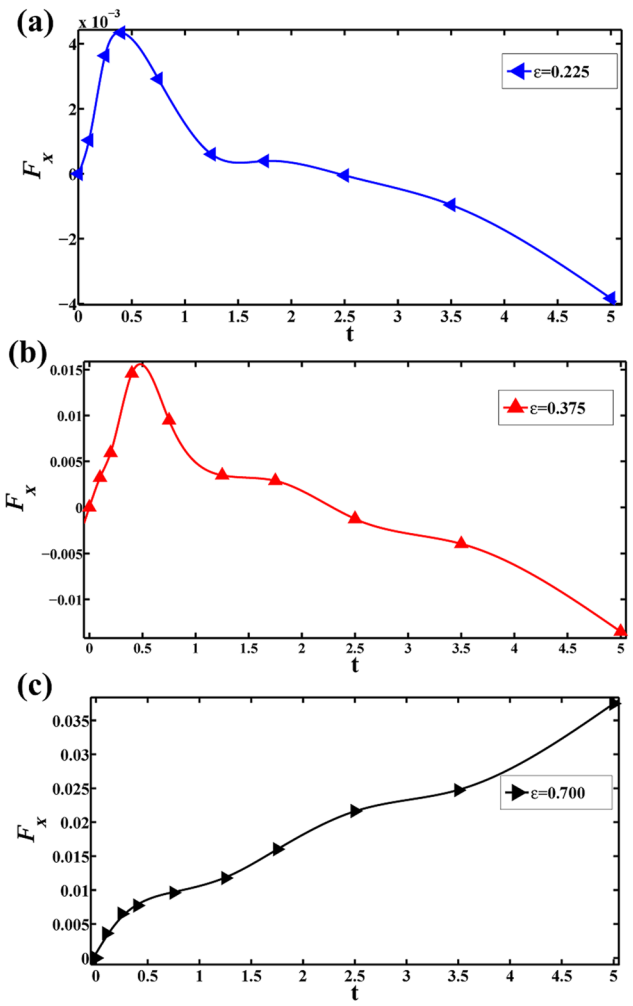

FIG. 13. The x component of the total drag force F_x *versus* time t for eccentric compound droplets with different initial eccentricities under initial $Ca = 0.20$. (a) ε = 0.225, (b) ε = 0.375, and (c) ε = 0.700.

The enhancing and suppressing effects of the inner droplet on the interfacial curvatures are also shown in Figs. 12(a)–12(c) which present the pressure curves of two endpoints of the eccentric compound droplets. For the three different initial eccentricities ε = 0.225 for Fig. 12(a), ε = 0.375 for Fig. 12(b), and ε = 0.700 for Fig. 12(c), the pressures at dot 1 are always higher than those at dot 2 in the BF stage and they are always lower in the AFUD stage. Thus, in the BF stage, the inner asymmetric pressure distribution will cause the right shift of the compound droplet, and in the AFUD stage it will cause the left shift. From these three figures, it could be seen that the pressure difference at two ends is always increasing when the inner droplet gets bigger.

Figure 13 exhibits the curves of the x component F_x of the total drag forces for three initial eccentricities. When ε = 0.225 and ε = 0.375, values of F_x are positive at first and increase along with time until reaching a maximum. Then, the curves will decline and might be negative in the AFCD stage. When ε = 0.700, values of F_x are much higher than those for ε = 0.225 and ε = 0.375 at most of the time. They are always positive and monotonously increasing. In the BF stage, the curve of F_x ascends rapidly; after the BF stage, values of F_x are relatively quite large and still increasing, but the slope becomes a little smaller. As we already knew, the outer drag is generally stronger to the half of the compound droplet in which the inner droplet is staying. Since the inner droplets always stay in the right half, the outer drags always tend to pull the compound droplet to the right in both BF and AFUD stages no matter how big the inner droplets are.

The time-evolution curves of the mass center of the compound droplets with inner droplets of different sizes are shown in Fig. 14, from which the common action of inner pressure differences and outer drag forces on the shift of the eccentric compound droplets could be seen. When ε = 0.225 and ε = 0.375 [see Figs. 14(a) and 14(b)], initially, the compound droplets shift to the right a little, which is caused by the positive common action of both the inner pressure differences and outer drag forces. Then, the curves of d descend continuously, which means that the compound droplets begin to shift to the left. At this moment, from Figs. 13(a) and 13(b) it could see that the outer drags pull the compound droplet to the right but from Figs. 12(a) and 12(b) the inner pressure differences move the compound droplet to the left. Thus, the left shifts of the eccentric compound droplets are caused by the inner pressure differences, i.e., by the interfacial curvature differences. When ε = 0.700 [see Fig. 14(c)], the d curve is always positive and ascends continuously although the ascending rates in different stages change a little bit. As shown in the inset of Fig. 14(c), the ascending rate in stage one is relatively high since both the inner pressure difference and the outer drag are positive to the right shift in this stage; in stage two and

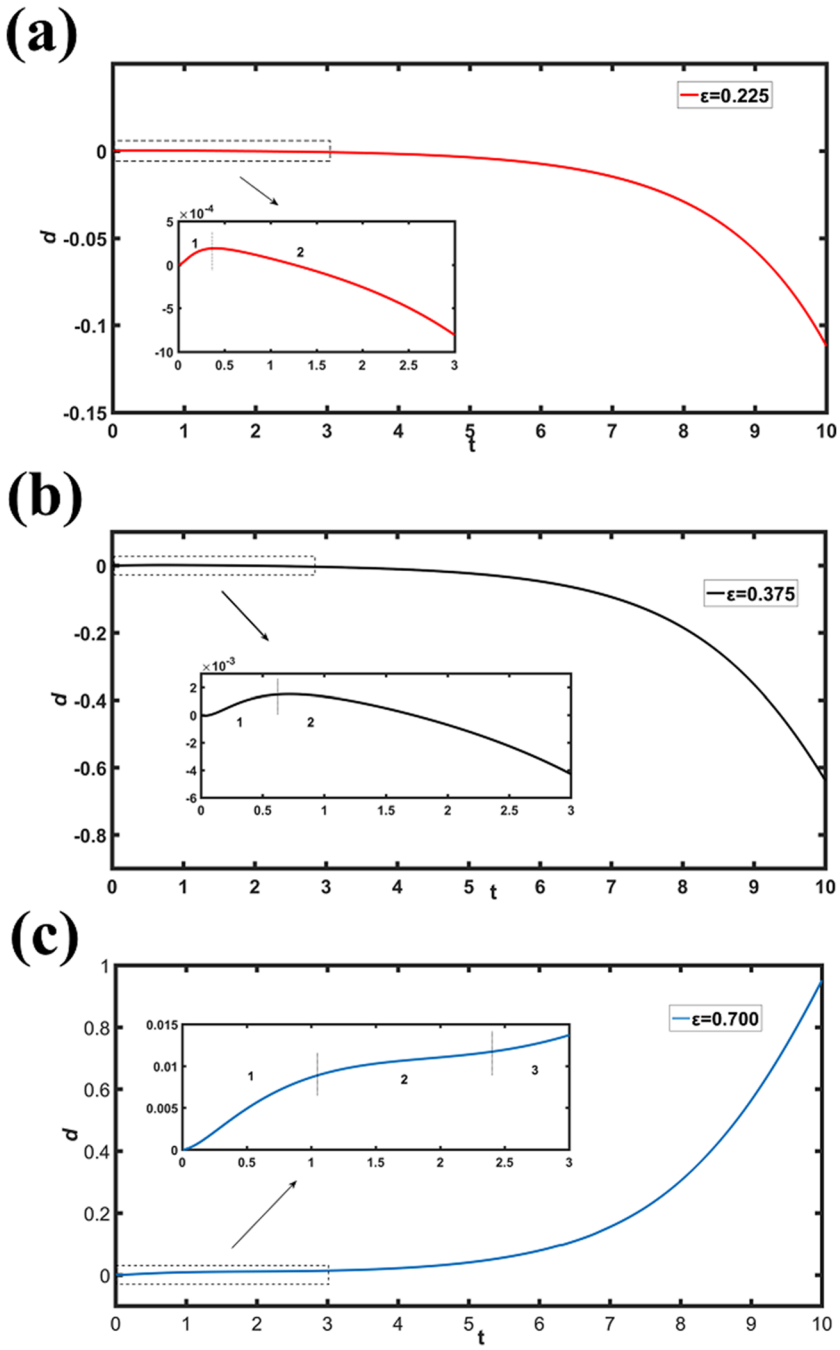

FIG. 14. The displacement d of the mass center of the eccentric compound droplets *versus* time t for various initial eccentricities under $Ca = 0.20$. (a) $\varepsilon = 0.225$, (b) $\varepsilon = 0.375$, and (c) $\varepsilon = 0.700$.

three, the outer drag is quite big and positive but the inner pressure difference is negative to right shift; as a result, the slope of d curve in this stage decreases a little. Thus, the right shift of the eccentric compound droplet is caused by the outer drag.

Comparing the results shown in Figs. 8–10 to those in Figs. 11–14, it could be seen no matter how generating the asymmetries either by changing the location or by the size, the mechanisms to cause the directional movement and inverse of eccentric compound droplets are the same. Besides Ca = 0.20, the cases when Ca = 0.22 has also been investigated in order to make the conclusion more convincing. As its results are very similar to those for Ca = 0.20, they are not shown here to avoid the lengthiness, but in the supplementary material.

IV. CONCLUSIONS

By investigating the rheological behaviors of eccentric compound droplets, whose asymmetries are generated by changing either the location or the size of inner droplets, in a modest extensional flow, the mechanical mechanisms of their directional movement and inverse have been investigated in this paper. According to the common sense, generally, the movement of a globule is driven by the asymmetric outer drags. However, in this work, a shift which is driven by the asymmetric interfacial curvature of the compound droplet is revealed. As the inner droplet has both enhancing and suppressing effects on the deformation of the compound droplet in different stages, the asymmetric layout of the inner droplet

leads to the asymmetric deformation of the compound droplet. Thus, the globule has different interface curvatures at two endpoints. This curvature difference results in the asymmetric pressure distribution and circulation inside the compound droplet, which could drive the globule shifting in some direction by changing its mass center. In addition, the internal asymmetry also results in the asymmetric outer drags from the continuous phase. Certainly, the asymmetric drag could drive the compound droplet shifting too. The higher the asymmetry is, the larger the outer drag is. The interaction between the outer (drags) and the inner (internal pressure differences) driving force causes the oriented shift and inverse of the compound droplet eventually. Thus, the shift direction is affected not only by the structural asymmetry parameter ε (eccentricity) but also through some flow features such as the capillary number. Changing these factors might cause the variation of the shift direction. When the initial ε and Ca are relatively small (below the critical curve of Ca), the compound droplet is mainly driven by the asymmetric interfacial curvatures and shifts to the left; when ε and Ca are relatively large (above the critical curve of Ca), the compound droplet is mainly driven by the outer drags and shifts to the right. When the capillary number Ca is increased, the flow shear gets stronger and naturally the effect of drags will becomes larger, which is consistent to our result and could explain that the droplet shifts to the right at the large Ca. The results obtained in this paper might have significant potential applications for the curvature-driving movement of soft globules.

SUPPLEMENTARY MATERIAL

See supplementary material for the case for Ca = 0.22 that has also been investigated in order to make the conclusion more convincing and the results that are shown from Figs. S1–S6.

ACKNOWLEDGMENTS

Supported by National Natural Science Foundation of China (Nos. 21576185 and 21376162).

[1] W. Wang, M. J. Zhang, and L. Y. Chu, "Functional polymeric microparticles engineered from controllable microfluidic emulsions," Acc. Chem. Res. **47**(2), 373–384 (2013).
[2] J. T. Wang, J. Wang, and J. J. Han, "Fabrication of advanced particles and particle-based materials assisted by droplet-based microfluidics," Small **7**(13), 1728–1754 (2011).
[3] H. S. Chen, J. Li, H. C. Shum, H. A. Stone, and D. A. Weitz, "Breakup of double emulsions in constrictions," Soft Matter **7**(6), 2345–2347 (2011).
[4] J. Li, H. S. Chen, and H. A. Stone, "Breakup of double emulsion droplets in a tapered nozzle," Langmuir **27**(8), 4324–4327 (2011).
[5] Y. P. Chen, X. D. Liu, C. B. Zhang, and Y. J. Zhao, "Enhancing and suppressing effects of an inner droplet on deformation of a double emulsion droplet under shear," Lab Chip **15**(5), 1255–1261 (2015).
[6] Y. P. Chen, G. Gao, C. B. Zhang, and Y. J. Zhao, "Three-dimensional splitting microfluidics," Lab Chip **16**(8), 1332–1339 (2016).
[7] H. A. Stone and L. G. Leal, "Breakup of concentric double emulsion droplets in linear flows," J. Fluid Mech. **211**(211), 123–156 (1990).
[8] H. C. Kan, H. S. Udaykumar, W. Shyy, and R. Tran-Son-Tay, "Hydrodynamics of a compound drop with application to leukocyte modeling," Phys. Fluids **10**(4), 760–774 (1998).
[9] E. M. Toose, B. J. Geurts, and J. G. M. Kuerten, "A 2D boundary element method for simulating the deformation of axisymmetric compound non-Newtonian drops," Int. J. Numer. Methods Fluids **30**(6), 653–674 (1999).
[10] K. A. Smith, J. M. Ottino, and M. Olvera de la Cruz, "Encapsulated drop breakup in shear flow," Phys. Rev. Lett. **93**(20), 204501 (2004).
[11] C. Zhou, P. Yue, and J. J. Feng, "Deformation of a compound drop through a contraction in a pressure-driven pipe flow," Int. J. Multiphase Flow **34**(1), 102–109 (2008).
[12] J. Tao, X. Y. Song, J. X. Liu, and J. T. Wang, "Microfluidic rheology of the multiple-emulsion compound droplet transiting in a contraction tube through a boundary element method," Chem. Eng. Sci. **97**(7), 328–336 (2013).
[13] J. T. Wang, X. D. Li, X. Y. Wang, and J. Guan, "Possible oriented transition of multiple-emulsion compound droplets with asymmetric internal structures in a microfluidic constriction," Phys. Rev. E **89**(5), 052302 (2014).
[14] J. T. Wang, J. X. Liu, J. J. Han, and J. Guan, "Effects of complex internal structures on rheology of multiple emulsions particles in 2D from a boundary integral method," Phys. Rev. Lett. **110**(6), 066001 (2013).
[15] J. T. Wang, J. X. Liu, J. J. Han, and J. Guan, "Rheology investigation of the compound droplet of multiple emulsions with complex internal structures through a boundary element method," Chem. Eng. Sci. **96**(96), 87–97 (2013).
[16] J. T. Wang, X. Y. Wang, M. Tai, and J. Guan, "Oriented shift and inverse of the daughter droplet due to the asymmetry of grand-daughter droplets of multiple emulsions in a symmetric flow field," Appl. Phys. Lett. **108**(2), 021603 (2016).
[17] X. F. Qu and Y. C. Wang, "Dynamics of concentric and eccentric compound droplets suspended in extensional flows," Phys. Fluids **24**(12), 123302 (2012).
[18] J. T. Wang and D. M. Yu, "Asymmetry of flow fields and asymmetric breakup of a droplet," Microfluid. Nanofluid. **18**(4), 709–715 (2015).
[19] D. M. Yu, M. M. Zheng, T. M. Jin, and J. T. Wang, "Asymmetric breakup of a droplet in an axisymmetric extensional flow," Chin. J. Chem. Eng. **24**(1), 63–70 (2016).
[20] I. Nitschke, A. Voigt, and J. Wensch, "A finite element approach to incompressible two-phase flow on manifolds," J. Fluid Mech. **708**, 418–438 (2012).
[21] S. Chen and H. Rui, "A node-centered finite volume method for a fracture model on triangulations," Appl. Math. Comput. **327**, 55–69 (2018).
[22] M. Sheikholeslami and H. B. Rokni, "Magnetic nanofluid flow and convective heat transfer in a porous cavity considering Brownian motion effects," Phys. Fluids **30**(1), 012003 (2018).
[23] M. Sheikholeslami and M. Seyednezhad, "Simulation of nanofluid flow and natural convection in a porous media under the influence of electric field using CVFEM," Int. J. Heat Mass Transfer **120**, 772–781 (2018).
[24] P. Dimitrakopoulos and J. T. Wang, "A spectral boundary element algorithm for interfacial dynamics in two-dimensional Stokes flow based on Hermitian interfacial smoothing," Eng. Anal. Boundary Elem. **31**(7), 646–656 (2007).
[25] J. T. Wang, J. J. Han, and D. M. Yu, "Numerical studies of geometry effects of a two-dimensional microfluidic four-roll mill on droplet elongation and rotation," Eng. Anal. Boundary Elem. **36**(10), 1453–1464 (2012).